Design of variable-stiffness robotic hand using pneumatic soft rubber actuators

Jun-ya Nagase[1], Shuichi Wakimoto[2], Toshiyuki Satoh[3], Norihiko Saga[1] and Koichi Suzumori[4]

[1] School of Science and Technology, Kwansei Gakuin University, 2-1 Gakuen, Sanda, Hyogo, 669-1337, JAPAN

[2] Research Core for Interdisciplinary Sciences, Okayama University, 3-1-1 Tsushima-naka, Okayama, Okayama, 700-8530, JAPAN

[3] Faculty of Systems Science and Technology, Akita Prefectural University, 84-4 Aza Ebinokuchi, Tsuchiya, Yurihonjo, Akita, 015-0055, JAPAN.

[4] Graduate School of Natural Science and Technology, Okayama University, 3-1-1 Tsushima-naka, Okayama, Okayama, 700-8530, JAPAN

E-mail: J.Nagase@kwansei.ac.jp

Abstract. In recent years, Japanese society has been aging, engendering a labor shortage of young workers. Robots are therefore expected to be useful to perform tasks such as day-to-day work support for elderly people. Particularly, robots that are intended for use in the field of medical care and welfare, are expected to be safe when operating in a human environment because they often come into contact with people. Furthermore, robots must perform various tasks such as regrasping, grasping of soft objects, and tasks using frictional force. Given these demands and circumstances, a tendon-driven robot hand with a stiffness change finger has been developed. The finger surface stiffness can be altered by adjusting the input pressure depending on the task. Additionally, it can change the coefficient of static friction by changing surface stiffness merely by adjusting the input air pressure. This report describes the basic structure, driving mechanism, and basic properties of the proposed robot hand.

1. Introduction

Recently, because of the rapid progression of aging and the decrease of young workers in Japan, robots are anticipated for use in nursing care and welfare services, performing rehabilitation and daily domestic tasks. Safety is a particularly important characteristic of robots for use in environments with humans. Moreover, when a robot hand supports the day-to-day life of humans, it must perform dexterous manipulation, grasping of soft objects, and tasks using frictional force.

Past studies of human-like robot hands have examined tendon-driven systems based on DC motors on the "back" of the hand or the arm, [1,2] or direct systems in which the actuator is implemented in the finger joints to increase a joint's DOF [3–5]. Some robot hands have been produced with a soft construction: one system uses McKibben artificial muscles [6,7], and one system use soft fingers made of silicone rubber [8,9]. Moreover, many prosthetic hands also have been developed [10-17] which is necessary to support the daily activities of amputated people.

Because these robot hands mentioned above can achieve such dexterous manipulation as humans, they might be able to regrasp, which is necessary in day-to-day support of humans. However, it is also needed in day-to-day work support to grasp soft objects such as a water-filled paper cup. In the case of these fingers, it is easy to transform their shape greatly to grasp such a soft object because the fingers consist of hard materials. They generate high surface pressure locally.

For soft objects that deform easily, it is effective to obtain the contact area by constructing the finger surface of flexible materials. For example, a finger consisting of Flexible Micro Actuator is made of soft rubber materials [8]. However, the finger softness causes difficulty of manipulation [18].

Therefore, for dexterous manipulation and grasping of soft objects, contradictory specifications are

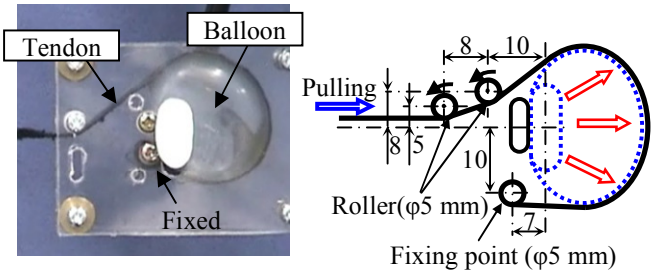

Figure 1 Tendon driven balloon actuator.

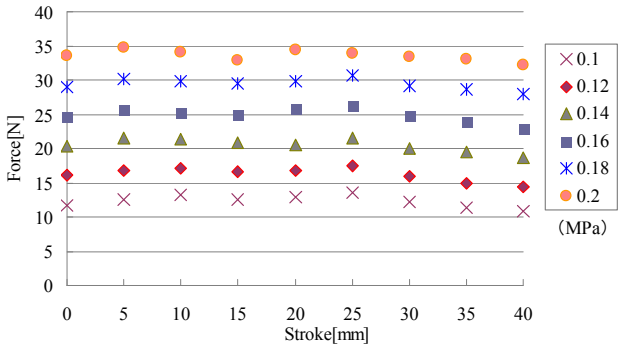

Figure 2 Relations between displacement and force on each pressure.

demanded for the finger. However, few robot hands satisfying those demands have been developed.

For day-to-day work support, there are also tasks using frictional force, such as the turning of pages. A finger developed by Murakami et al. [19] has achieved page-turning capability using frictional force produced by deforming rubber arranged on the finger surface. Slip motion of fingers is one task demanded in the day-to-day work support of humans. However, the finger surface softness engenders slip difficulty. In such cases, hardness is necessary. However, robot hands with variable finger hardness have been developed only to a slight degree.

In light of those studies and their outcomes, the purpose of this study is to resolve the problem of such contradictory demand specifications about dexterous manipulation and grasping of soft objects, tasks using frictional force, and slip motion. In this study, to resolve such a problem, a pneumatic robot hand with variable stiffness fingers that can change their softness and friction were developed. This report describes the design, driving mechanism, and fundamental characteristics of our proposed robot hand.

2. Pneumatic tendon-driven balloon actuator

2.1 Construction and Mechanism

The appearance and mechanisms of the balloon actuators are portrayed in Fig. 1. The balloon actuator [20] has an air-pressure-drive type actuator comprising a

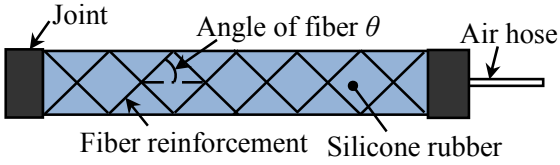

Figure 3 Structure of variable stiffness device.

silicone oval tube and tendon. The silicone rubber tube is sealed at one end to produce a balloon. Compressed air is supplied through an opening at the other end to expand the balloon. The tube is then fixed at both ends by acrylic plates. The wall is arranged on one side of the balloon to restrain its expansion. To decrease the loss of the output efficiency, a roller is arranged in the part where the tendon direction is changed. A basic driving mechanism is presented in Fig. 1. The tendon wrapped around the balloon is expanded when the balloon expands, which creates tensile force for the tendon drive.

2.2 Fundamental characteristic

Fundamental characteristics of the balloon actuator are presented in Fig. 2. This figure shows the relation between the generated force and strokes of tendon that are fixed at 0–40 mm per 5 mm. The input pressure is 0.1 MPa to 0.2 MPa per 0.02 MPa.

Consequently, the balloon actuator can output a stroke of more than 40 mm, and the generated force is about 35 N in spite of low pressure, for which the maximum input pressure is 0.2 MPa. In this study, the finger is driven by the generated force of a balloon actuator installed in the palm.

3. Pneumatic variable-stiffness finger

3.1 Variable-stiffness device

3.1.1 Structure and Mechanism

Fig.3 depicts the structure of variable-stiffness device [21]. This device consists mainly of silicone rubber, fiber reinforcement, and a joint part. The fiber reinforcement is inserted in the silicone rubber in a mesh-like pattern like the McKibben-type artificial muscle actuator [22]. The mechanism of the variable stiffness device is explained in this chapter as follows.

Generally, the diameter d of the McKibben-type artificial muscle actuator after its contracting is given as

$$d = d_0 \frac{\sin\theta}{\sin\theta_0} \quad (1)$$

Where θ is angle of fiber, The sign with index 0 is the value when the actuator is initial state. The fiber angle in expanding of the actuator is indicated in Fig.4. This figure shows the parallelogram “ABCD” consisting of

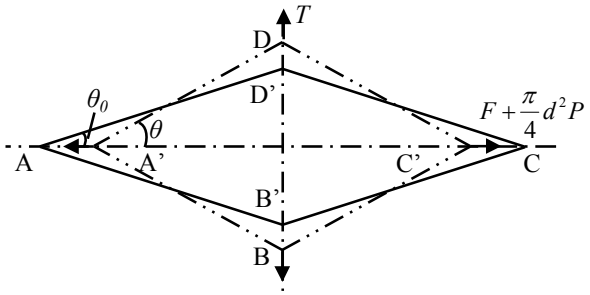

Figure 4 Fiber angle in expanding of the actuator.

the fiber. The parallelogram shifts from "ABCD" to "A'B'C'D'" by contacting of the actuator. Therefore the following equations are true.

$$\frac{L_0}{\cos\theta_0} = \frac{L}{\cos\theta} \tag{2}$$

$$\cos\theta = \frac{L}{L_0}\cos\theta_0 = (1-\varepsilon)\cos\theta_0 \tag{3}$$

$$\sin\theta = \sqrt{1-(1-\varepsilon)^2\cos^2\theta_0} \tag{4}$$

The equation that the equation (1) is substituted for eq. (4) is as follows.

$$d = \frac{d_0}{\sin\theta_0}\sqrt{1-(1-\varepsilon)^2\cos^2\theta_0} \tag{5}$$

When the tension force for circumference direction of the actuator is given as T, The following equation is true.

$$\left(F + \frac{\pi}{4}d^2P\right)\tan\theta = T \tag{6}$$

The force for the radius direction acting on minute part is given as follows.

$$P\frac{d}{2}d\phi \tag{7}$$

Moreover, the total value of the vertical component of the radius direction's force can be expressed as follows.

$$2T = 2\int_0^{\frac{\pi}{2}} P\frac{d}{2}\sin\phi d\phi = Pd \tag{8}$$

Consequently, the contraction force F is given as follows from eq. (5),(6) and (8).

$$F = \frac{\pi {d_0}^2 P}{4\sin^2\theta_0}\left\{3(1-\varepsilon)^2\cos^2\theta_0 - 1\right\} \tag{9}$$

McKibben-type artificial muscle actuator begins to contraction when compressed air is provided to the actuator. Then the contraction force is decrease by increasing the contraction. The contraction ratio, when the contraction force becomes 0, indicates the ε when F is 0 in the next eq. (10).

$$\varepsilon = 1 - \frac{1}{\sqrt{3}\cos\theta_0} \tag{10}$$

From eq. (10), when the angle of fiber θ_0 is 54.7 deg, the contraction ratio is 0. In this manner, when

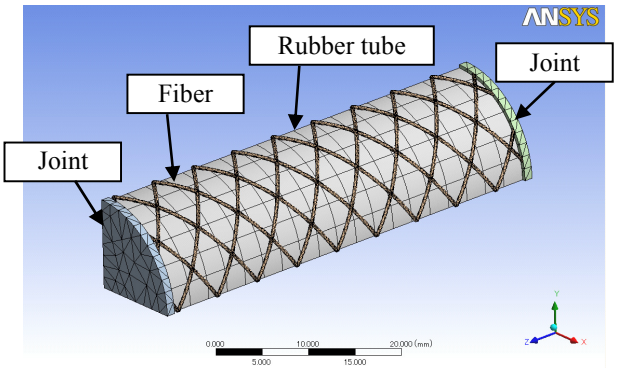

Figure 5 The 1/4 FEM analysis model of the variable stiffness device.

Table 1 FEM analysis conditions.

	rubber tube	fiber	joint
Element type	Hexahedron	Tetrahedron	Tetrahedron
Young's modulus	3.0MPa	1.0×10^4MPa	2.1×10^5MPa
Poisson's ratio	0.45	0.3	0.3
Number of nodes	926	19467	1470
Number of elements	114	7598	340
Analysis method	Newton-Raphson method		
Analysis option	Large deformation analysis		

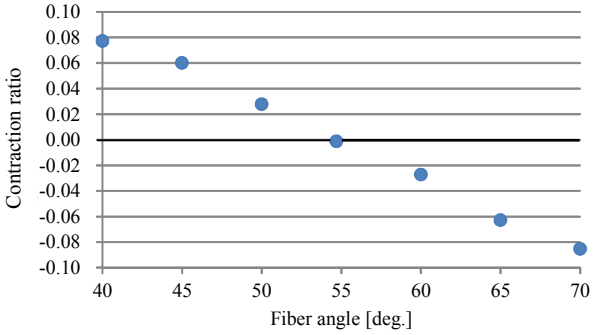

Figure 6 Relation between fiber angle and contraction ratio.

compressed air is provided to the device, only its rigidity and stiffness are changed without contraction and expansion.

3.1.2 FEM analysis

From eq. (10), ideal fiber angle, leading $\varepsilon = 0$, can be obtained as 54.7 deg. However this equation was derived under these assumptions; the length of rubber tube is infinity, and elastic force of the rubber is ignored. Therefore to clear the adequateness of the equation and the influences of these assumptions, FEM analysis is carried out.

FEM analysis model used in this study is show in Fig.5. This model is 1/4 model of the variable stiffness device that the diameter is 20mm and the length is 50mm in initial state. The air pressure is 0.2MPa because calculation errors occur in case of higher

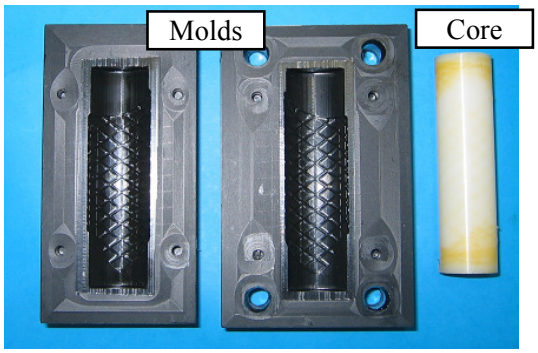

Figure 7 Molds with spiral convex structure and cylindrical core for making variable stiffness device.

pressure. And, fiber angle θ_0 is set as 40, 45, 50, 54.7, 60, 65 and 70 deg. . In the analysis, the displacement of one end of the model is fixed for all direction, and that of another end of the model is fixed for only radius direction. Moreover, the inside of the model is given the pressure that is 0.2MPa. The analysis' condition is shown in Table 1. In this analysis, because the purpose is to evaluate qualitatively the influence on contraction ratio of fiber angle, the material of the rubber is assumed the linear material.

Analysis results measured the relationship between fiber angle and contraction ratios are shown in Fig.6. In case of 54.7deg, analysis result of ε is almost zero compared with other fiber angle, and it is ignorable in practice usage. Therefore we decided the fiber angle is 54.7deg.

3.1.3 Fabrication of the variable-stiffness device

The variable stiffness device is fabricated by pouring room temperature vulcanized (RTV) silicone rubber in molds. Fig.7 portrays the molds and a cylindrical foundry core for producing the device. Molds have a convex shape part for making grooves of the rubber surface to arrange fibers with an angle of 54.7 deg.

The cylindrical core is put between two molds. Then RTV silicone rubber in a liquid state is poured into them. After heating by 80°C for 20 min, it reaches an elastic state. Then, it is reinforced by 16 fibers. The 104-μm-diameter Kevlar fiber material has high tensile strength. The reinforced tube part with the cylindrical core is put to other molds that have no convex shape; silicone rubber is poured again to cover them thinly. Using this manufacturing method, fibers are not exposed on the device surface. The rubber thickness is 1.5 mm, with outer diameter of 20 mm.

3.2 Design of the variable-stiffness finger

3.2.1 Structure and driving mechanism

Fig. 8 depicts the structure of the variable stiffness finger. Each finger segment consists mainly of the variable-stiffness device. The input pressure for this

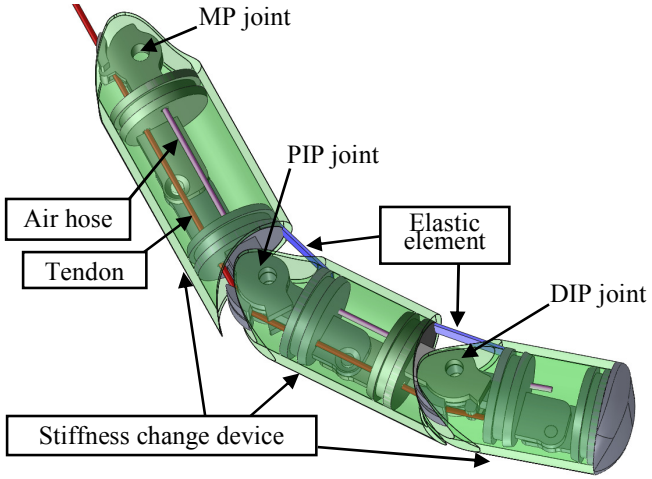

Figure 8 Structure of a stiffness change finger.

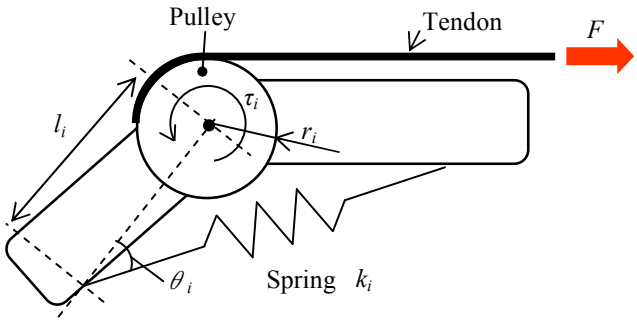

Figure 9 Diagram of the joint of fingers.

device is provided via the inside of the silicon tube of 1 mm diameter installed inside the device. Tendons are connected to the DIP joint and MP joint through the interior of the device. The elastic elements are arranged in each joint.

Therefore, the finger flexes by restoring the force of the elastic elements and extends it by tensile force of the balloon actuator, which is aimed at preventing the fall of an object because the grip force can be secured if the system stops abnormally.

The joint mechanism is inserted inside of each stiffness change device. Consequently, the device does not warp even if the robot hand grasps a heavy object, and the device can grasp it while transforming it along the shape of the object.

3.2.2 Grasping trajectory

Because the finger tendons are connected to the DIP joint and MP joint, the MP joint can be moved for independence and the DIP joint operates simultaneously with the PIP joint. This driving structure is the same as that of a human hand. Therefore, not only grasping but also pitching is possible using the proposed robot hand.

The finger is designed so that it flexes in order of the MP joint, PIP joint, and DIP joint to contact along the object when grasping. Fig. 9 depicts a diagram of the *i*-

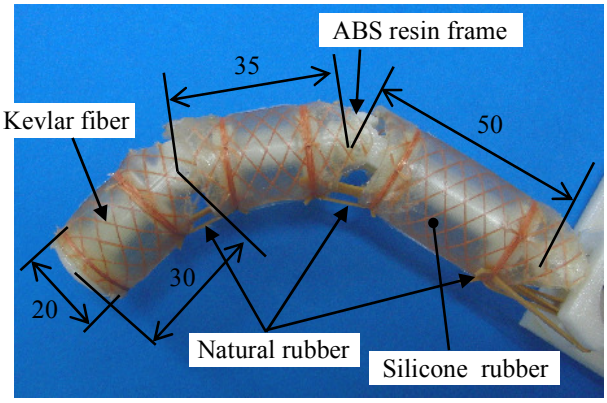

Figure 10 Prototype of a stiffness change finger.

th joint of the finger. In this diagram, the joint torque τ_i is as shown in eq. (2)–(4). Consequently, the spring constant of elastic elements and radius of the pulleys are decided using these equations.

$$\tau_i = \tau_{ai} - \tau_{bi} \quad (2)$$

$$\tau_{ai} = l_i \cdot k_i \cdot \delta_i \cdot \sin\theta_i \quad (3)$$

$$\tau_{bi} = F \cdot r_i \quad (4)$$

In those equations, τ_i is the torque acting on the joint, τ_{ai} is the torque by restoring the force of the elastic element, τ_{bi} is the torque generated by force of the balloon actuator, l_i signifies the distance from the pulley center to the spring edge of the fingertip side, k_i stands for the spring constant of the pulling spring, δ_i represents the growth from the natural length of the spring, θ_i denotes the angle between the straight line that links the spring edge of the fingertip side to the pulley center and the straight line that linked both ends of the spring, F represents the generated force of the balloon actuator, and r is the pulley radius. If $\tau_{a3} > \tau_{a2} > \tau_{a1}$ and $\tau_{b3} = \tau_{b2} = \tau_{b1}$, then τ_a is greater than τ_b in the order of the MP joint, PIP joint, and DIP joint, then the finger flexes from the root toward the tip of the finger when the force of the balloon actuator is decreased. The robot hand can thereby grasp and hold an object in one movement. The spring constant of each spring is chosen such that the torque is greater in order of the MP joint, PIP joint, and DIP joint. The spring specification is decided as follows: the DIP joint is 0.8 N/mm, the PIP joint is 1.2 N/mm, and the MP joint is 1.8 N/mm. Additionally, each pulley's radius is 5 mm.

3.2.3 Prototype of finger

Fig. 10 presents the finger prototype. The size of a finger is almost identical to that of a finger of a human hand. The silicone rubber thickness for the variable stiffness device is 1.5 mm; Kevlar fiber is inserted inside of the rubber as a fiber reinforcement. The elastic elements arranged in each joint are made of natural rubber. Furthermore, 1-mm-diameter silicone tubes are

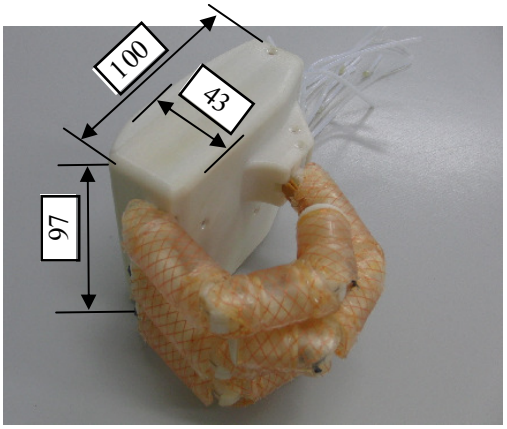

Figure 11 Prototype of the proposed robot hand.

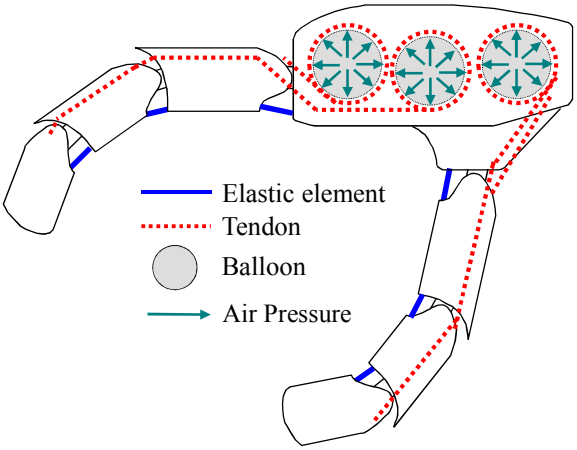

Figure 12 Structure of the proposed robot hand.

installed inside the device. The air pressure is provided to the device through the interior of that tube. The finger frame is made of ABS resin. All parts except the metal wire as a tendon of 0.3 mm diameter are made from non-metal material. Therefore, the finger is lightweight: 0.02 kg.

4. Robot hand with a variable-stiffness finger

4.1 Construction and driving mechanism

Fig. 11 presents a photograph of the robot hand prototype with a variable stiffness finger. Fig.12 shows an internal structure of the robot hand. Table 2 presents the developed robot hand's specifications. The robot hand fingers are 4 in all, with 3 joints per finger, making 12 in all. Degrees of freedom of joints are 2 per finger, making 8 in all. The robot hand size is almost identical to that of a human hand.

Eight balloon actuators are installed in the palm of the robot hand. Six balloon actuators are for fingers, and two balloon actuators are for a thumb. An actuator is used for MP joint per finger, and another actuator is also used for PIP joint and DIP joint per finger. These

Table 2 Specifications of proposed robot hand

Total weight[kg]	0.27		
Weight of a finger[kg]	0.02		
Diameter capacity[mm]	160		
Weight capacity[kg]	0.5		
Number of joints	12		
Degree of freedom	8		
Number of actuatrs	8		
Material of frame	ABS resin		
	DIP	PIP	MP
Output torque[Nmm]	50	80	140
Operating angle[deg.]	0~75	0~75	0~75

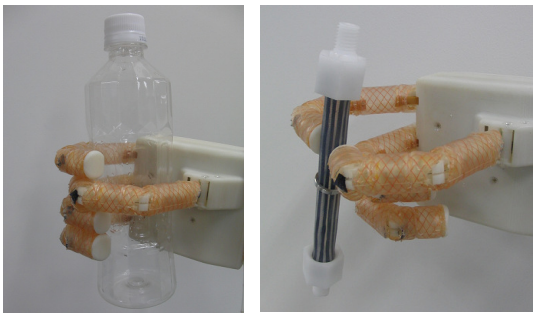

(a) Grasping (b) Pinching

(c) Platform

Figure 13 Grasping various objects by proposed robot hand.

fingers can be controlled individually. The robot hand generates grasping force by restoring force of elastic element and decreases it by tensile force of the balloon actuator as shown Fig.12.

Figure 13 presents the grasping states of several objects. Grasping, pitching, and platform are possible using this proposed robot hand. The robot hand frame is made of ABS resin. Its total weight is 0.27 kg, which is lighter than a human hand.

4.2 Evaluation of fundamental characteristics

Because we assume that the proposed robot hand is applied to day-to-day work support, it must be able to grasp soft objects. Therefore, it is effective to obtain the contact area to consist the surface of fingers in flexible materials. However, the finger surface softness causes difficulty of manipulation.

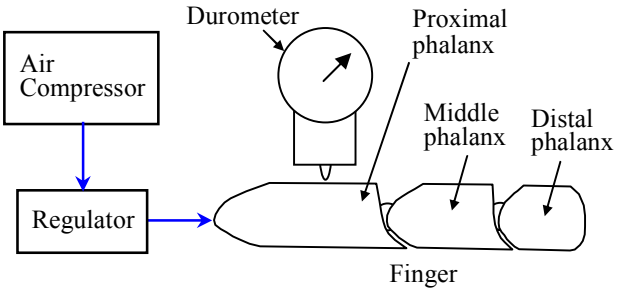

Figure 14 Experimental set-up for measurement of stiffness characteristics

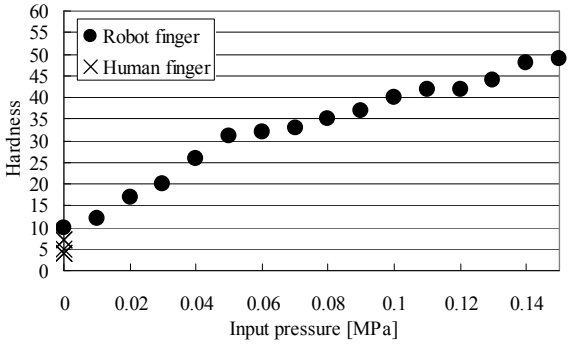

(a) Distal phalanx

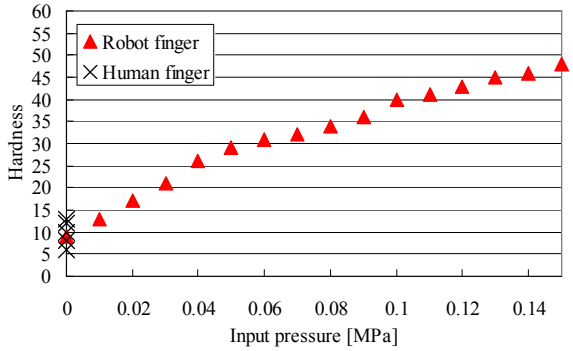

(b) Middle phalanx

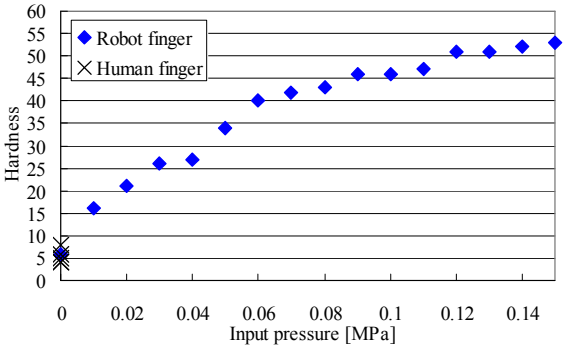

(c) Proximal phalanx

Figure 15 Stiffness characteristics of proposed finger.

By making the finger a variable-stiffness device, the robot hand can grasp a soft object easily and can manipulate objects easily with high dexterity by adjusting the finger softness. This robot hand can also

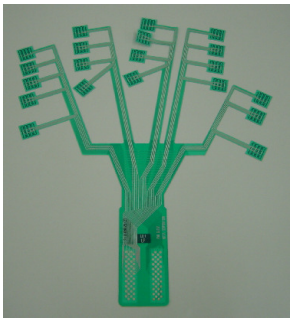

(a) Tactile sensor

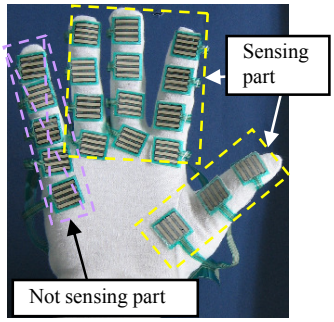

(b) State arranged in hand

Figure 16 Experimental setups for measuring the pressure distribution.

Table 3 Contact area and total force of human and robot hand.

Subject		Contact area (mm^2)	Total force (N)
Human hand		721	7.3
Robot hand	0MPa	684	10.1
	0.15MPa	302	9.0

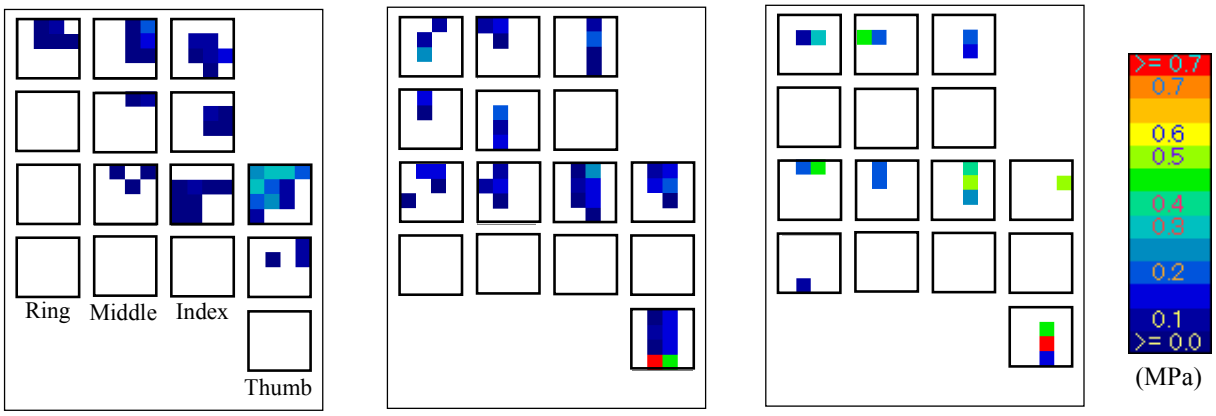

(a) Human hand

(b) Robot hand (Input pressure is 0MPa)

(c) Robot hand (Input pressure is 0.15MPa)

Figure 17 Grasping pressure distributions of a human and robot hand.

adjust the frictional force by changing the input pressure. Therefore, we think it can turn pages easily and perform slip motions smoothly such as rubbing of the human body.

Consequently, in this chapter, the evaluation of fundamental characteristics is performed to confirm its effectiveness as a robot hand that can execute such various tasks.

4.2.1 Stiffness characteristics

To evaluate stiffness characteristics, the surface stiffness of each finger device is evaluated according to its hardness, as measured using a rubber hardness tester (Durometer E, WR-107E; WESTOP). The human finger is also measured. Fig.14 presents the experimental setup. In the experiment, when the input pressure is set at 0–0.15 MPa per 0.01 MPa, the device hardness is measured. In a human hand, the respective hardnesses of each segment of the index fingers of five people were measured using the tester.

Fig. 15 presents results of hardness measurements of each segment. The figure shows that the robot finger hardness is less than 10 when the input pressure is 0 MPa. When the input pressure is 0.15 MPa, which is the maximum pressure in this experiment, the hardness is about 50.

Comparison of the finger hardness of 0 MPa with that of a human finger highlights their similarity. For that reason, it indicates the surface stiffness of the finger can be changed by adjusting the input pressure. The proposed robot finger has equivalent surface stiffness to that of a human finger when the input pressure is 0 MPa.

4.2.2 Pressure distribution characteristics

The grasping pressure distribution characteristics were evaluated to elucidate the effectiveness of the finger consisting of a soft silicone rubber tube. The pressure distribution characteristics were measured when the robot hand grasp objects were measured using a tactile sensor (I-SCAN; Nitta Corp.). The pressure distribution of the human hand finger was measured using the same method as that of the robot hand.

Fig. 16 presents the experimental setup. The tactile sensor consists of a sensor sheet, cuff unit, and computer. The sensor sheet has electrodes in the x-axis direction and y-axis direction, respectively. The electrode is coated with a special ink. When pressure is

generated in the sensor sheet, the resistance of that special ink changes depending on the pressure. Then, the cuff unit receives this change of resistance as a change of electrical current. The cuff unit has an A/D converter and multiplexer circuit; it converts the change of pressure into a digital signal. Then the computer collects the change of pressure through the cable. The sampling frequency is 60 Hz.

In the experiment, after the robot hand and human hand grasp the cylindrical object for which the diameter is 88 mm, height is 115 mm, and weight is 0.1 kg, the grasping distribution pressures are measured using a tactile sensor that is arranged in both the robot hand and human hand, respectively. Input pressures to the variable stiffness devices are, respectively, 0 MPa and 0.15 MPa.

Table 3 presents the contact area and total contact force of the robot hand and human hand. Fig.17 represents their pressure distribution.

First, we specifically examine the experimentally obtained result of the robot hand. The total force when input pressure is 0 MPa is 10.1 N and that when input pressure is 0.15 MPa is 9.0 N.

These values have few differences. However, the contact area when input pressure is 0 MPa is 684 mm^2; that when the input pressure is 0.15 MPa is 302 mm^2. Consequently, the contact area when the input pressure is 0 MPa is greater than twice that when the input pressure is 0.15 MPa. This result indicates that the finger consisting of soft silicone rubber can produce contact areas that are greater than twice those of a hard finger. As shown in Fig. 17, although the grasping pressure is greater than 0.5 MPa in many areas when the input air pressure is 0.15 MPa, it is less than 0.3 MPa in almost all areas except the root of the thumb when the input air pressure is 0 MPa. Furthermore, the contact area of the robot hand when the input air pressure is 0 MPa is similar to that of the human hand: that of the robot hand is 684 mm^2; and that of the human hand is 721 mm^2.

4.2.3 Friction characteristics

The proposed robot hand can grasp objects flexibly, similarly to a human hand when the input air pressure is 0 MPa. It is sure to perform dexterous manipulation and slip motion easily by the decreasing coefficient of friction when the input air pressure is high. Therefore, we believe that the robot hand can turn pages and rub the human body smoothly.

In an earlier study, Sugano [23] developed a finger with finger tip curvature that differs at each point. This finger's frictional force is adjusted by changing the contact area when changing the contact point. Murakami [19] developed a finger for which the rubber

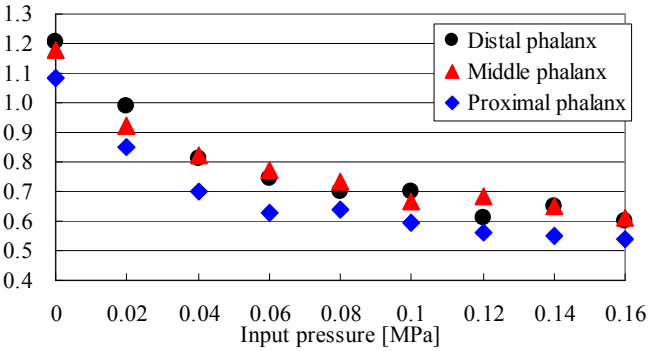

Figure 18 Friction characteristics of proposed finger.

is arranged on the surface. Its frictional force can be changed by changing the contact area when changing the contact force. This finger can be adjusted to the coefficient of static friction; it has achieved turning of pages. To change the frictional force, the user must adjust the finger tip posture of, and must later adjust the contact force to objects. Therefore, these fingers are changed passively according to the frictional force.

For our proposed finger, the frictional force is changed actively. By changing the finger surface stiffness, the frictional force can be adjusted by changing contact area, and does not require adjustment of the finger posture and contact force. Therefore, for instance, when the finger rubs the human body, it might be moved smoothly on the body without giving unpleasantness to the human by keeping the contact force and finger posture.

There, we examined the coefficient of static friction of the finger by experimentation to confirm whether the finger changes the coefficient of friction by changing of the surface stiffness. In this experiment, at first, the weight of 0.2 kg is put on the variable stiffness device that is put on the horizontal stand. Second, the device is inclined slowly. Third, the angle at which the weight starts to slip on the device is measured. Finally the coefficient of static friction is calculated using the angle. The experiment is performed when the input air pressure to the device is 0–0.16 MPa per 0.02 MPa.

Fig. 18 represents experimentally obtained results. These values are the averages of measured values. As a result, the coefficient of friction is changed by input air pressure in every finger segment, and is higher with decreasing air pressure. We believe that the coefficient of friction of this finger depends mainly on the contact area. In addition, the range of the frictional coefficient of each finger segment is the following: the distal phalanx and the middle phalanx are about 0.6–1.2; the proximal phalanx is about 0.55–1.1 from Fig.18. Based on the above result, we confirmed that the coefficient of

static friction of the proposed finger can be adjusted without changing the finger posture and contact force.

5. Conclusion

This report described the design, driving mechanism and fundamental characteristics of the proposed robot hand with a variable-stiffness finger. Our conclusions are the following.

(1) The developed finger consists of silicone rubber, fiber reinforcement, and the ABS resin material. The weights of the robot hand and its finger are about 0.27 kg and 0.02 kg, respectively, which are lower than those of a human hand. The proposed robot hand can perform grasping, pitching, and platform functions.

(2) The softness and friction coefficient of the proposed finger can be changed easily by adjusting the input air pressure to the variable-stiffness finger devices.

(3) The finger can change softness by changing the input air pressure. When the input air pressure to the finger is 0 MPa, the robot hand can grasp objects flexibly, like a human hand. In this experiment, we confirmed that the proposed robot hand can have a contact area similar to that of a human hand. When the input air pressure to the finger is 0.15 MPa, it might perform dexterous manipulation comparatively easily because the finger hardness improves the manipulation performance [15].

(4) The coefficient of static friction of the finger can be changed by changing the surface stiffness by adjusting the input air pressure. This experimentally obtained result suggests that the robot hand is able to turns page and rub a human body smoothly by changing the friction coefficient. However, to perform rubbing, evaluation of the coefficient of dynamic friction is necessary. Therefore, we will examine it as a subject of future work.

Acknowledgement

This research was supported by "Grant-in-Aid for Young Scientists (B) (No. 23760246)".

References

[1] Butterfass J, Grebenstein M, Lieu H and Hirzinger G 2001 DLR-Hand II: Next Generation of a Dextrous Robot Hand *Proc. 2001 IEEE Int. Conf. on Robotics and Automation* pp 109–14

[2] Lovchic C S and Diftler M A 1999 The Robonaut Hand: A Dexterous Robot Hand for Space *Proc. 1999 IEEE Int. Conf. on Robotics and Automation*, pp 907–12

[3] Jacobsen S C, Iversen E K, Knutti D F, Johnson R T and Biggers K B 1986 Design of the Utah/MIT Dexterous Hand 1986 *Proc. 1986 IEEE Int. Conf. on Robotics and Automation* pp 1520–32

[4] Yamano I, Takemura K and Maeno T 2003 Development of a Robot Finger for Five-fingered Hand using Ultrasonic Motors *Proc. 2003 IEEE/RSJ Intl. Conf. on Intelligent Robots and Systems* pp 2648–53

[5] Kawasaki H, Shimomura H and Shimizu Y 2001 Education-al-industrial complex development of an anthropomorphic robot hand 'Gifu hand' *Adv. Robotics* **15** 357–63

[6] http://www.shadow.org.uk/products/newhand.shtml

[7] http://www.festo.com/cms/en-gb_gb/5001.htm

[8] Suzumori K, Iikura S and Tanaka H 1992 Applying a Flexible Microactuator to Robotic Mechanisms *IEEE Control Systems* **12** 21–27

[9] Noritsugu T, Kubota M and Yoshimatsu S 2001 Development of Pneumatic Rotary Soft Actuator Made of Silicone Rubber *J. Robotics and Mechatronics* **13** 17–22

[10] Zollo L, Roccella S, Guglielmelli E, Carroza M C, and Dario P, 2007 Biomechatronic design and control of an anthropomorphic artificial hand for prosthetic and robotic application, *IEEE/ASME Trans. Mechatronics* **12** 418–428

[11] Controzzi M, Cipriani C, and Carrozza M C 2008 Mechatronic design of a transradial cybernetic hand *Proc. 2008 IEEE/RSJ Int. Conf. Intell. Robots Syst.* pp 576–581

[12] Kargov A, Pylatiuk C, Oberle R, Klosek H, Werner T, Roessler W, and Schulz S 2007 Development of a multifunctional cosmetic prosthetic hand *Proc. 2007 IEEE 10th Int. Conf. Rehabil. Robot.* pp 550–553

[13] Jung S and Moon I 2008 Grip force modeling of a tendon-driven prosthetic hand *Proc. Int. Conf. Control Autom. Syst.* pp 2006–2009

[14] Light C M and Chappel P H 2000 Development of a lightweight and adaptable multiple-axis hand prosthesis *Med. Eng. Phys.* **22** 679–684

[15] Kyberd P J and Pons J L 2003 A comparison of the oxford and manus intelligent hand prostheses *Proc. 2003 IEEE Int. Conf. Robot. Autom.* pp 3231–3236

[16] Huang H, Jiang L, Liu Y, Hou L, and Cai H 2006 The mechanical design and experiments of HIT/DLR prosthetic hand *Proc. 2006 IEEE Int. Conf. Robot. Biomimetics* pp. 896–901.

[17] http://www.touchbionics.com/

[18] Takeuchi H and Watanabe T 2010 Development of a Multi-fingered Robot Hand with Softness-changeable Skin Mechanism *Proc. 41st Int.*

Symposium on Robotics and Sixth German Conf. on Robotics pp 606–12

[19] Murakami K and Hasegawa T 2003 Novel fingertip equipped with soft skin and hard nail for dexterous multi-fingered robotic manipulation *Proc. 2003 IEEE Int. Conf. on Robotics and Automation*, pp 708–13

[20] Saga N, Nagase J and Kondo Y 2006 Development of a Tendon-Driven System Using a Pneumatic Balloon *J. Robotics and Mechatronics* **18** 139–45

[21] Wakimoto S, Kumagai I and Suzumori K 2009 Development of large Intestine Endoscope Changing Its Stiffness *Proc. of 2009 IEEE Int. Conf. on Robotics and Biomimetics* pp 2320–25.

[22] Schulte H F 1961 The Characteristics of the McKibben Artificial Muscle *The Application of External Power in Prosthetics and Orthetics* 94–115

[23] Morita T, Iwata H and Sugano S 2000 Human Symbiotic Robot Design based on Division and Unification of Functional Requirements *Proc. 2000 IEEE Int. Conf. on Robotics and Automation* pp 2229–34